HEAT PUMP, SOLAR ENERGY AND ICE STORAGE SYSTEMS - MODELLING AND SEASONAL PERFORMANCE

Christian Winteler, PhD., Research Associate,
University of Applied Sciences and Arts Northwestern Switzerland,
Institute of Energy in Building,St. Jakobs-Strasse 84, 4132 Muttenz, Switzerland
Ralf Dott, Dipl.-Ing. RWTH, Research Associate,
University of Applied Sciences and Arts Northwestern Switzerland,
Institute of Energy in Building, St. Jakobs-Strasse 84, 4132 Muttenz, Switzerland
Thomas Afjei, Prof. Dr.sc.techn. ETH, Head of Building Technology Group,
University of Applied Sciences and Arts Northwestern Switzerland,
Institute of Energy in Building,St. Jakobs-Strasse 84, 4132 Muttenz, Switzerland
Bernd Hafner, Dr. rer. nat, Research Department,
Viessmann Werke GmbH & Co KG, 35107 Allendorf, Germany

Abstract: This paper investigates the seasonal performance of a combined solar, heat pump and ice storage system for residential dwellings. Simulation models for an ice storage and a solar thermal absorber are presented and compared to test data. A simulation study is performed for four different heat loads, i.e. building types, ranging from low-energy building to non-renovated existing building. The simulation results show that the solar ice storage system generates heat efficiently for a large variety of heat loads and consistently reaches a seasonal performance factor comparable to heat pump systems with borehole heat exchangers, i.e. SPF ~ 4.

Key Words: heat pumps, ice storage, solar thermal, combined systems

1 INTRODUCTION

The turnaround in energy policy demands energy supply systems to use predominantly renewable energy sources. Heat pumps in combination with solar energy are key technologies for heat generation for space heating and domestic hot water in buildings. Currently the most effective heat sources for heat pumps are borehole heat exchangers. Recently systems with large ice storages have been promoted as equally efficient at comparable cost without the need for deep drilling and the associated authorization and risks. Furthermore, ice storages can also be installed in areas where deep drilling is not possible or prohibited, even in water protection areas since the ice storage is filled with pure water.
Aim of this study is to investigate the seasonal performance of a combined solar, heat pump and ice storage system. First, specific components models for the ice storage and the solar absorber are presented and compared to test data. In a simulation study the seasonal performance of the heat generation system is determined for buildings with different heat loads and compared to the average seasonal performance factor of systems with borehole heat exchangers of ~ 4.0.

2 METHODS

The work presented here is conducted as simulation study. Figure 1 shows a schematic representation of the solar ice heat generation system. The central component is a brine/water heat pump that supplies heat for space heating, as well as for domestic hot water (DHW) preparation. The primary source of the heat pump is an unglazed solar absorber that generates heat from solar irradiation as well as from convective gains. A buried ice storage serves as alternative heat source for the heat pump in case the absorber cannot supply the necessary heat. In the ice storage heat is predominantly stored as latent heat, i.e. in the phase transition from water to ice. Excess heat from the absorber is used to recharge the ice storage. Additionally, the ice storage also gains heat from the surrounding soil. As soon as all the water in the ice storage is turned into ice and more heat is extracted, the temperature in the ice storage rapidly drops. In this case, the source temperature of the heat pump drops below the operational limit of the heat pump (usually around -10 °C) and the heat pump shuts off. Heat supply is then provided by an electric backup heater.
The simulation models of the ice storage and the unglazed solar absorber have been developed further in the course of this work. A detailed description of these models and a validation with field test or laboratory data will be presented in the following section. All other system components have already been validated with laboratory and field test data.
Heat generated by the heat pump is used for space heating (SH) and DHW preparation of a single family house (SFH). Heat pump models intended by the manufacturer for the solar ice storage system have thermal capacities of 6, 8, 10 and 13 kW. Therefore four reference buildings with corresponding heat loads (including DHW preparation) were defined and discussed in detail in Winteler et al. 2014. These buildings are labeled SFH25, SFH45, SFH60 and SFH100 where SFH stands for single family house and the numbers refer to the space heat demand in kWh/m^2/a.

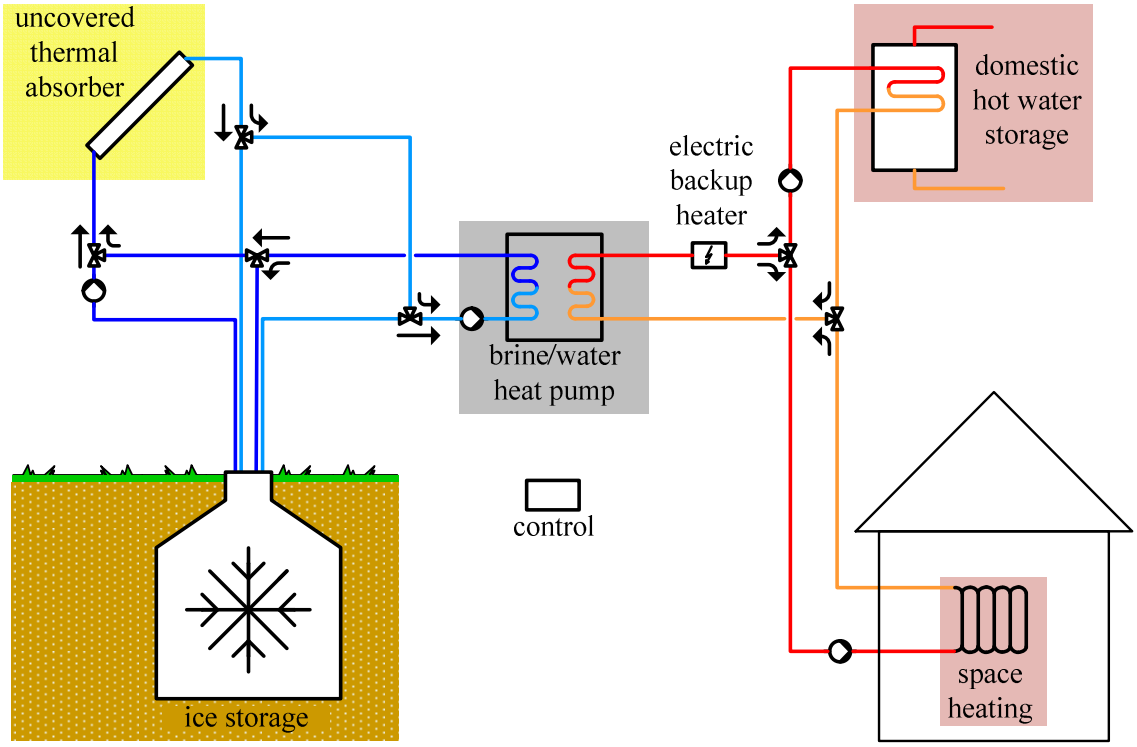

Figure 1: System and hydraulic scheme of the solar and ice storage heat generation system.

2.1 Ice Storage

The ice storage is an underground water tank that serves as heat source for a heat pump that in turn provides heat for SH and DHW preparation. Heat can be extracted effectively from the ice storage until all the water inside has turned into ice. Since temperature does not change during the phase change from liquid to solid, the source temperature for the heat pump stays constantly around the freezing-point. The freezing is interrupted by phases of regeneration, where heat from solar absorbers or from the surrounding soil is introduced into the ice storage. Due to the low temperature in the ice storage, the solar absorbers can be used for regeneration already at low ambient temperature. During the warm summer months, when only little energy is needed for SH and solar heat is abundant, the ice in the ice storage is completely melted and the water heated to around 25 °C. Thus the ice storage is a seasonal storage for solar and ambient heat. The combination of heat pump with seasonal storage and solar absorber could provide a viable alternative to systems with borehole heat exchangers where drilling is prohibited or uneconomical. Since the ice storage is filled solely with water, it could also be installed in water protection areas.

2.1.1 Ice storage model

The simulation model for the ice storage is meant to represent the Isocal SolarEis System. Its main component is a cylindrical concrete cistern filled with 10 m^3 of water. The tank is not insulated and therefore thermally connected to the surrounding soil. Heat extraction and regeneration is performed with PE-pipe heat exchangers that are arranged in several layers inside the tank. The power characteristic of the heat exchangers is determined experimentally. Ice formation on the heat exchanger pipes is not modelled directly, but it is assumed that the reduction in thermal transmittance due to the ice is compensated for by the increasing heat exchanger surface.
The ice storage itself is modeled as lumped capacitance, i.e. the temperature inside the ice storage is assumed to be homogeneous. Since temperature does not change during the phase change, the temperature inside the ice storage cannot be determined with a heat balance equation. Instead, the enthalpy of the water inside the tank is calculated from the enthalpy balance

$$\dot{h}_{H_2O} = \frac{1}{m_{H_2O}} \cdot \sum \dot{Q} \tag{1}$$

where $\sum \dot{Q}$ is the sum of all energy changes due to heat extraction or introduction and m_{H_2O} the mass of water inside the tank. In order to solve the differential equation (1), the initital value for the enthalpy has to be calculated according to

$$\boldsymbol{h_{H_20,init} = (1 - f_{ice}) \cdot q_{f,ice} + \Theta(-f_{ice}) \cdot c_{p,H_2O} \cdot T_{init}.} \tag{2}$$

Here f_{ice}, the initial fraction of ice inside the tank, and T_{init}, the initial temperature of the storage content in °C, are user-defined initial parameters. $q_{f,ice}$ is the specific heat of freezing water-ice and c_{p,H_2O} is the specific heat capacity of water. $\Theta(x)$ is the Heaviside step function whose value is zero for negative argument and one for positive argument.
Once the enthalpy is known, the water (ice) temperature can be estimated by linear interpolation on the values in Table 1, where $c_{p,ice}$ denotes the specific heat capacity of ice.

Table 1: Interpolation table for temperature calculation.

Enthalpy [J/kg]	$-10 \cdot c_{p,ice}$	$-3 \cdot c_{p,ice}$	$q_{f,ice}$	$10 \cdot c_{p,H_2O} + q_{f,ice}$
Temperature [°C]	-10	-3	0	10

2.1.2 Ground heat coupling

Heat exchange with the ground surrounding the ice storage can be an important source of regenerative heat as soon as the ice storage temperature drops below soil temperature. A schematic depiction of the ground heat exchange model is given in Figure 2. The ground temperature is assumed to correspond to the undisturbed ground temperature. In order to account for the interaction between tank and soil, especially the feedback from tank to soil, a cylindrical soil layer around the bottom part of the tank is modeled as lumped capacitance. This soil layer acts as thermal resistance between undisturbed ground and storage tank and is referred to as disturbed ground. Furthermore, the tank wall acts as additional thermal resistance between disturbed ground temperature and ice storage content.

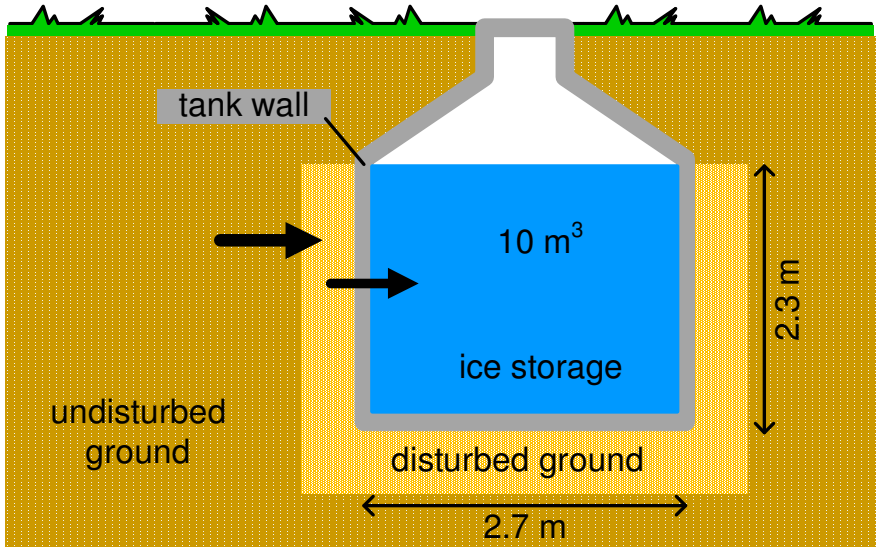

Figure 2: Schematic depiction of the ice storage model including soil model for ground heat exchange

2.1.3 Validation/Comparison with field measurement data

The ice storage model, including the ground heat exchange model, was validated using field measurement data. Unfortunately, some technical problems occurred during data taking which lead to incomplete data and several periods without reasonable data, sometimes for several consecutive days. Due to simplifications in the model and the aforementioned problems while data taking, the validation was limited to a plausibility check of storage temperatures and energy balance. The simulation setup for validation consisted of the ice storage model and a simulation model of the heat pump that was used in the field test building. Measurement data of the heat contribution from the solar absorber was directly fed into the ice storage model. Since the storage temperature cannot be measured directly, a lower and upper limit was estimated from measurement data. The temperature of the storage outlet to the solar absorber gives an upper limit of the ice storage temperature, whereas the outlet temperature to the heat pump serves as lower limit. A comparison of simulation and measurement data is given in Figure 3**.**
Simulation and measurement started on January 1st and stopped in mid-august. Except for the period between day 50 and day 125, the simulated ice storage temperature agrees very well with the limits derived from measurement. In general, the simulated temperatures are close to the lower observational limit.

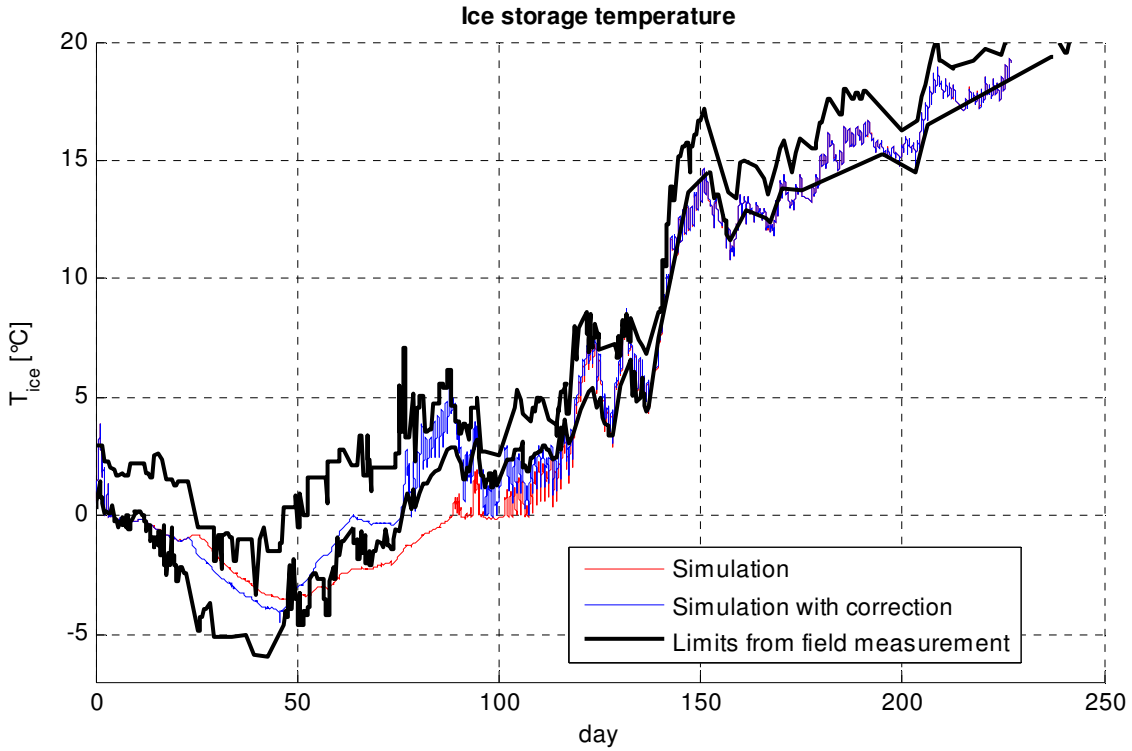

Figure 3: Comparison of simulated ice storage temperature and limits derived from field measurement data.

The period where simulation and measurement do not agree corresponds to the period when the ice storage is thawing i.e. the ice is melting. Considering that measurement data is fragmented during this period, especially in the heat contribution from the absorber, the resulting simulated temperature is qualitatively still in good agreement with measurements. To investigate whether the simulation model would stay within the limits from field measurements if continuous data was available, corrections were introduced when data was missing. The resulting temperature curve is shown as blue line in Figure 3. The agreement with measurement data during freezing and thawing is much better and the simulated temperature stays mostly within the observational limits.
Under the given circumstances – simplicity of the simulation model and fragmentation of measurement data – the simulation model yields plausible results. However, it has to be noted that the model is not universally valid but limited to this specific build of ice storage. Furthermore, the assumption that the reduction in thermal transmittance due to the ice is compensated for by the increasing heat exchanger surface seems to be valid but needs to be validated in more detail for future simulations.

2.2 Unglazed Solar Absorber

The main purpose of the solar absorber in the presented heat generation system is to serve as heat source for the heat pump. In addition, excess heat is stored in the ice storage. Both the heat pump and the ice storage only need energy at a temperature level below 20 °C. Therefore, an unglazed solar absorber is used. The advantage of an unglazed collector is, that if the operating temperature of the absorber is below ambient temperature not only absorption of solar irradiation can be used as heat source but also the enthalpy of ambient air via convection. In some cases, when the temperature of at least parts of the absorber surface is below the dew point temperature, even heat gains from condensation can be used.

2.2.1 Absorber simulation model

The simulation model of the unglazed absorber represents an Isocal SLK-S pipe absorber consisting of two layers of PE-pipes. The unglazed absorber is modeled as 2xN-nodes model. The 2 nodes are the absorber surface temperature on one hand and the temperature of the heat transport fluid on the other. Both are split up into N nodes in flow direction. A detailed description of the model can be found in Frank 2007. The model equation is given as

$$\dot{q}_{use} = \dot{q}_{abs} + \dot{q}_{conv,gain} - \dot{q}_{conv,loss} - \dot{q}_{sky} - c_{eff}\frac{\partial T_f}{\partial t}. \quad (3)$$

It takes into account solar gains from absorption of direct and diffuse irradiation, convective gains and losses as well as losses due to long wave radiation emission to the sky. The last term accounts for the effective thermal capacity of the absorber. While the model itself could also include heat gains from condensation, there was no data available to determine the corresponding coefficients. Therefore, condensation effects are currently not taken into account.

2.2.2 Validation with laboratory measurement data

Parameter identification and model validation were performed based on laboratory performance measurements. Measurements were taken at three different wind speeds with and without irradiation. To account for the influence of wind speed, coefficients for convective gains and losses, as well as the collector efficiency are split up into a constant and a wind dependent part. The fit parameters for convective gains can be determined from measurements without irradiation

$$\dot{q}_{conv,gain} = C_{gain} \cdot (T_m - T_a) = (C_{0,gain} + v_{wind} \cdot C_{1,gain}) \cdot (T_m - T_a), \quad (4)$$

where T_m is the mean absorber temperature and T_a the ambient Temperature. To determine the linear fit coefficients $C_{0,gain}$ and $C_{1,gain}$ the combined coefficient was fitted for every wind speed individually. The wind speed dependence was than derived by linear regression analysis. The resulting power curves are shown in Figure 4. It was stated in the measurement report, that there is currently no general equation available for the thermal performance without irradiation. Therefore a polynomial fit (dashed line) was given together with measurement

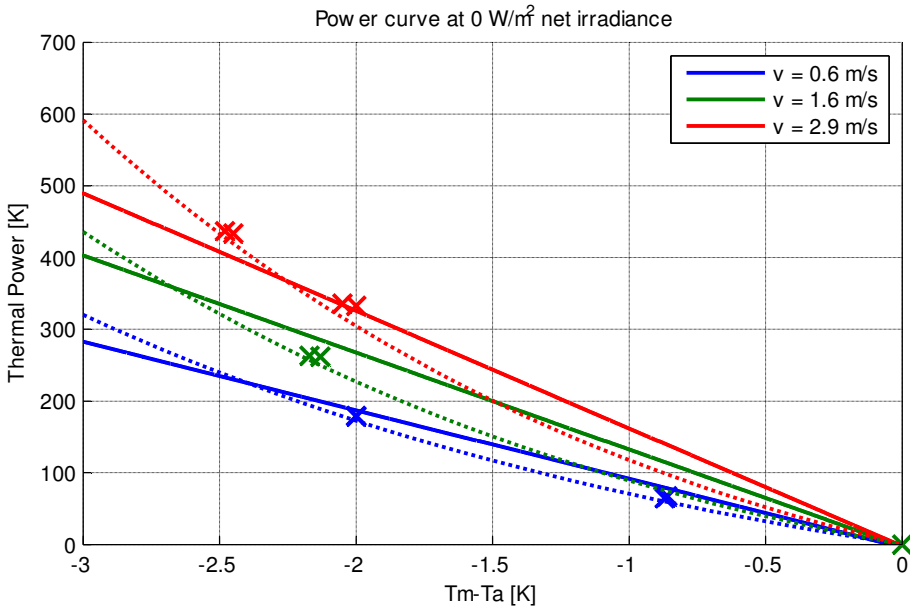

Figure 4: Thermal power curves for test without irradiance and three different wind speeds. Measurement points are marked with an 'x', dashed lines indicate a polynomial fit and the results from the simulation model are shown as solid line.

data (x). It was also stated that because of the test setup, negative temperature differences above 2.5 K are not possible to achieve. Since the absorber will not be used for cooling in our simulations, we only considered negative temperature differences. Even though only a handful of data points are available, the linear fit (solid line) shows a reasonably good agreement with measurement data.
From measurements with irradiation, the absorber efficiency and convective heat loss coefficients can be derived simultaneously.

$$\dot{q}_{abs} = \eta \cdot I = (\eta_0 + v_{wind} \cdot \eta_1) \cdot I \tag{5}$$

$$\dot{q}_{conv,loss} = C_{loss} \cdot (T_m - T_a) = \left(C_{0,loss} + v_{wind} \cdot C_{1,loss}\right) \cdot (T_m - T_a) \tag{6}$$

Again, the combined coefficient was individually fitted for every wind speed and the wind speed dependency derived a posteriori by linear regression. The resulting power curves are plotted in Figure 5. Together with the measurement data, the laboratory report contained a first-order fit that is shown in Figure 5 as dashed lines. The power curves obtained from the simulation model are in very good agreement with the results from laboratory measurements. The absolute difference between simulated power and the fitted laboratory data is always less than 10 W.

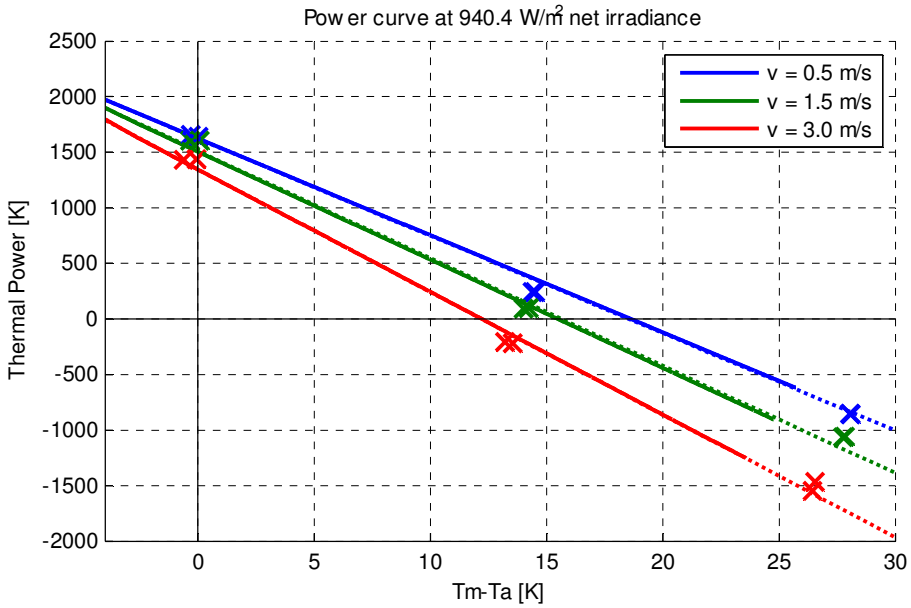

Figure 5: Thermal power curves for test with irradiance and three different wind speeds. Measurement points are marked with an 'x', dashed lines indicate a first order fit given in the test protocol and the results from the simulation model are shown as solid line.

3 SIMULATION STUDY

All simulations are performed with MATLAB®/SIMULINK® in combination with the CARNOT Blockset, an extension for the calculation and simulation of thermal components of heating systems. All simulation results are annual values from July to July with 300 days preconditioning, corresponding to one full heating period. Heat loads are simulated with the simple house model from the CARNOT Blockset parameterized such according to the building definitions from [ref SHC paper]. The Isocal solar ice system consists of Isocal SLK-S pipe absorber modules and an Isocal SES ice storage.
The absorber is modeled as described in the previous chapter and parameterized according to manufacturer data. For the brine/water heat pump the generic heat pump model from the CARNOT Blockset is used with performance data of Viessmann Vitocal 300 G BW series models BW 301.A06 (6 kW), BW 301.A08 (8 kW), BW 301.A10 (10 kW) and BW 301.A13 (13 kW). The storage tank model is a CARNOT multiport model with specifications of a Viessmann Vitocell 100-V CVW. All simulation models and applied parameter data sets have furthermore been validated through field test measurement data.

2.3 Reference conditions

The reference conditions described in Dott et al. 2011 and Haller et al. 2011 are applied for all building types using the following options and modifications:

- Moderate climate of Wuerzburg, a German city in central Europe.
- Domestic hot water preparation is delivered by a boiler with attached mixing valve to adjust the fixed tapping temperature and heated only by the heat pump. Storage temperature is set to 50 °C. For small storages (≤ 400 l) water circulation and renewal is assumed to be sufficient to prevent pathogen growth (Legionella).
- The seasonal variation of the DHW energy demand is approximated by a sine-curve variation of the cold water temperature around a mean value of 10 °C with amplitude 3 °C and phase shift -137 days.
- Simplified DHW tapping profile of only three tappings per day (07:00, 12:00 and 19:00) corresponding to an average draw off of 200 l/d at 45 °C or 7.964 kWh/d (2907 kWh/a).
- The heat delivery system for space heating in SFH25, SFH45 and SFH60 is a floor heating system, in SFH100 a radiator. The required flow temperatures needed to satisfy the heat demands at design outdoor temperature are 30 °C for the SFH15 building, 33 °C for the SFH45, 41°C for the SFH60 building and 48 °C for the SFH100 building. Mass flows are determined as ratio of design heat load and design temperature differential times heat capacity (cf. Table 2).
- The heating characteristic of the heat pump controller defines the space heating return flow temperature as a function of the outdoor temperature. The heating characteristic is set such that the room temperature is kept around 20 ± 0.5 °C. If necessary, DHW preparation has priority over space heating.
- Solar thermal absorber modules are installed on a south facing roof at an inclination of 40°.
- The collector area amounts approximately to 10 m^2 for SFH25, 13 m^2 for SFH45, 20 m^2 for SFH60 and 30 m^2 for SFH100.
- Internal heat gains are approximated by a constant heat gain of 2.6 W/m2.
- Heat losses through the ground floor are calculated using a constant soil temperature of 10 °C.

4 RESULTS

The System boundary for the performance factor calculation includes all components of the system excluding the heating and DHW distribution systems. Figure 6 shows a visualization of the energy flows and the system boundary. The system boundary corresponds to *system boundary bSt – before storage* according to the definitions in Malenkovic et al. 2012. It is a measure for the performance of the system without the influence of storage losses and the energy distribution system, which is generally different for every installation site and cannot be influenced by the manufacturer or installer of a SHP system (Malenkovic et al. 2012).
The corresponding seasonal performance factor is labeled **SPF_{bSt}** and is defined as:

$$SPF_{bSt} = \frac{\int \left(\dot{Q}_{HP,SH} + \dot{Q}_{HP,DHW} + \dot{Q}_{BU,SH} + \dot{Q}_{BU,DHW} \right) \cdot dt}{\int \left(\sum P_{el,SHP} \right) \cdot dt} \text{, with} \quad (7)$$

$$\sum P_{el,SHP} = P_{el,sol} + P_{el,HPSrc} + P_{el,HP} + P_{el,BU} + P_{el,CTRL} \quad (8)$$

A selection of results for the three chosen systems is presented in Figure 7 and Table 2. Therein, the following results are shown:

- The total generated heat for space heating and domestic hot water preparation in kilowatt-hours (kWh), divided into the different heat sources for the heat pump: electricity, solar collector or ice storage. The contribution from the ice storage is subdivided into a solar and a ground heat part, depending on how the heat extracted from the ice storage is restored. Since heat exchange between ice storage and ground works in both ways, the displayed value denotes the net annual energy balance. The latent heat contribution cannot be displayed here since its annual energy balance is zero.
- The seasonal performance factor SPF_{bSt} of the heat generation system according to Eq. 7.

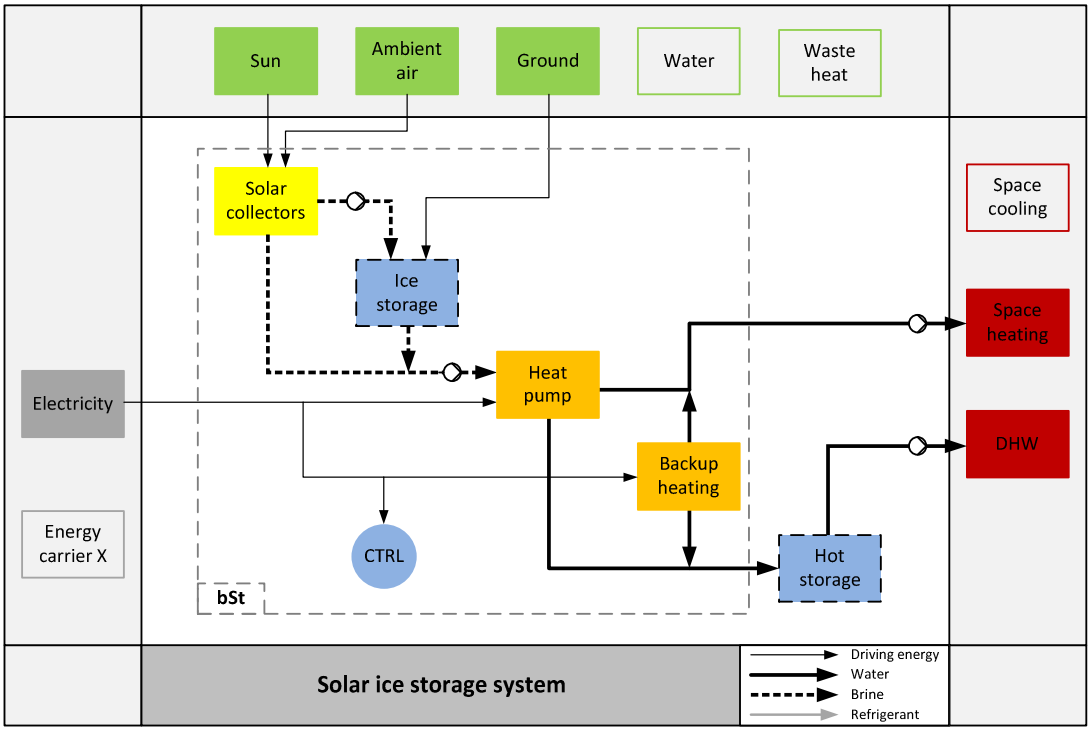

Figure 6: Visualization of the energy flows of the solar ice storage heating system. The dashed square indicates the system boundary for the calculation of the SPF. The representation method is based on [10].

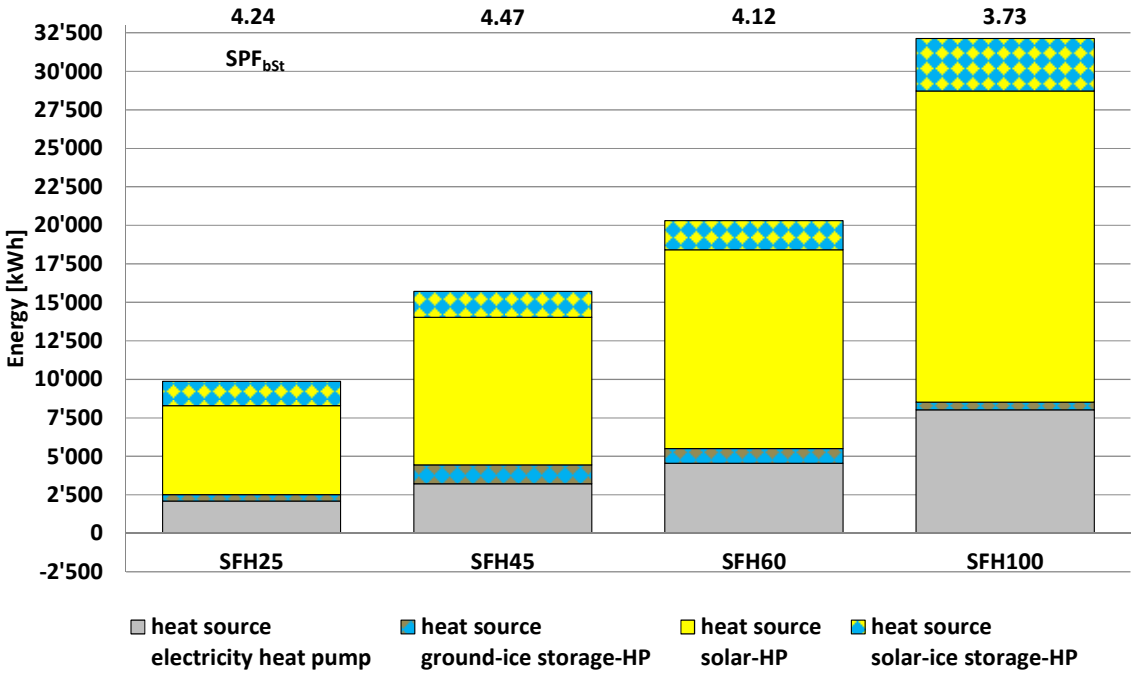

Figure 7: Annual energy balance of the heat generation system (heat pump, solar collector and ice storage).Usable energy is depicted on the ordinate axis, subdivided into the different heat sources of the heat pump. Negative values indicate a net heat loss from the ice storage to the ground.

For most building types, a system configuration could be found that yields $SPF_{bSt} > 4$. Only for the building types with the highest (SFH100) and the lowest (SFH15) heat demand the desired SPF_{bSt} could not be reached. Various factors that have a negative effect on the efficiency in these systems will be discussed in the next section.
The breakdown of heat pump heat sources in Figure 6 shows that the predominant source in all systems is the solar collector. Heat extracted from the ice storage is also chiefly regenerated by the collectors; the net ground heat contribution is usually significantly lower than the aforementioned contributions.
Component dimensions are listed in Table 2. Due to the very high heat demand of the SFH100 variant, a second ice storage had to be installed to ensure heat generation without the need for direct electric backup heating throughout the year.

Table 2: System simulation results

Building type	Design heat load in kW	Solar absorber area in m^2	Thermal power of heat pump in kW	Total generated heat in kWh	Design flow/return temperature in °C	Total generator electricity consumption in kWh	SPF of heat generator
SFH25	5.5	10	6	9'558	30/25	2'254	4.24
SFH45	7.5	13	8	15'257	33/28	3'413	4.47
SFH60	9.5	20	10	19'784	41/31	4'800	4.12
SFH100	12.5	30	13	31'439	48/38	8'428	3.73

5 DISCUSSION

The simulation study yields good seasonal performance factors for all system configurations. Since the direct electric backup heater is very inefficient in generating heat, it should be used as little as possible or better not at all. In all presented simulations the electrical heater was never in use which in turn is an indicator that the source temperature of the heat pump was always above the operational limit. It also suggests, that the water in the ice storage was never completely frozen.
Due to the high insulation quality of building type SFH25, relatively little heat is needed for space heating and in turn the share of heat generated for DHW preparation is relatively high, around 30 %. Since significantly higher temperatures are needed for DHW preparation than for space heating, this has a lowering effect on the SPF. In addition, the electricity consumption of auxiliary systems (control, solar pump and heat pump source pump) is about equal for all three building types, but due to the low heat production for SFH25, there the negative effect on the SPF is much larger.
For the building type with radiator heating system (SFH100) flow and return temperatures are higher than for floor heating systems. This in turn leads to a reduction of the SPF. In addition, the higher the thermal power of the heat pump, the higher source mass flow rates are needed. To provide these mass flow rates more powerful pumps are needed which also consume more electric energy and therefore the SPF is reduced.
A detailed graphical unraveling of the heat pump heat sources is shown in Figure 7. The solar absorbers are the primary heat source for the heat pump in all simulations. Since the absorber area is in general increasing with increasing heat pump capacity, also the heat contribution from the absorbers is increasing. In contrast, the fraction of heat extracted from the ice storage that is regenerated with solar is roughly proportional to the size of the ice storage.
The contribution from the ground is significantly lower than the solar contribution to the ice storage and it varies much more among the different simulations. Since heat exchange with the ground works in both directions, the annual energy balance only shows half the picture.
Figure 8 shows the monthly energy balance of the ice storage in the SFH45 simulation. From May to October the ice storage is warmer than the surrounding ground and loses heat to the ground. At the same time the highest solar gains occur, but are almost completely lost to the

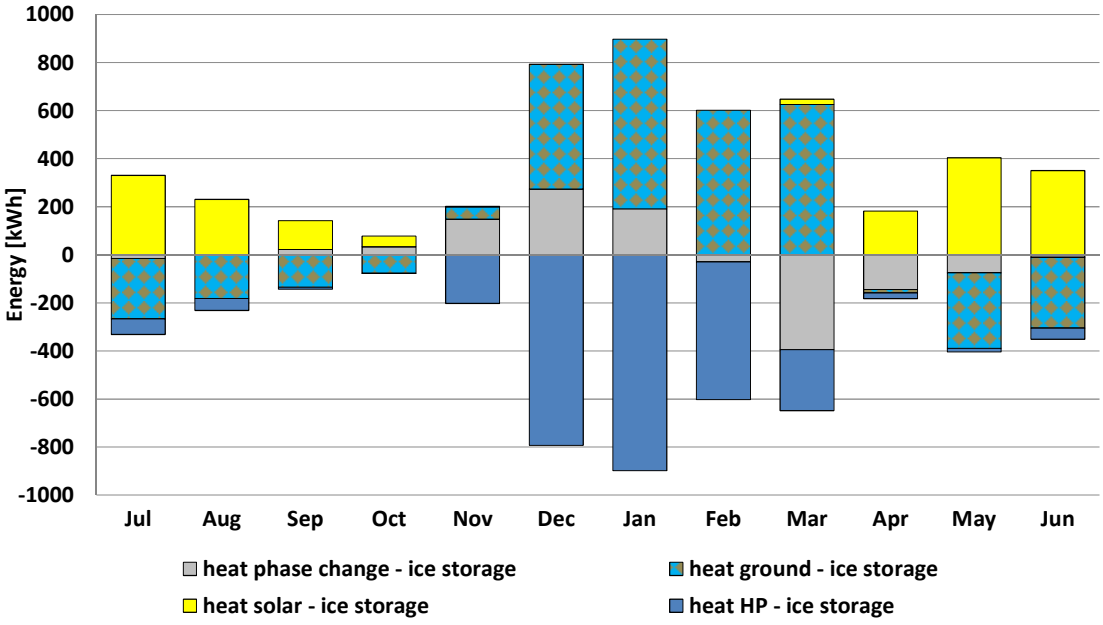

Figure 8: Monthly energy balance of the ice storage of simulation SFH45. Heat exchange is depicted on the ordinate axis, subdivided into the different exchange partners. Positive values indicate heat flow to the ice storage. Phase change gains (losses) describe energy released (lost) through cooling (heating) or freezing (thawing) of water/ice.

ground except for some heating of the water occurring in May. At the beginning of the heating period (October until March), the ice storage is quickly cooled below ground temperature (in October and November) resulting in heat gains from the ground during the rest of the period. While latent heat is extracted from November to January, thawing already starts in February and ends somewhere around April. Outside the heating period, only little heat is extracted from the ice storage by the heat pump.

6 CONCLUSION

Simulation models for an ice storage and an uncovered thermal absorber were presented and their validation results showed good agreement with field measurement or laboratory measurement data. Specific building models for the ice storage heating system simulated. The simulation study shows, that the solar ice system generates heat efficiently for different heat loads and under different climatic conditions. It reaches $SPF_{bSt} > 4$ for buildings with moderate (SFH25) to high (SFH100) space heat demands with space heating or radiator heat delivery systems.
Solar heat is the primary heat source for the heat pump. The ice storage stores solar heat and serves as source for the heat pump during the heating period. Heat exchange with the ground plays an important role in preventing complete freezing of the ice storage in winter and the resulting need for inefficient direct electric heating. We expect to be able to compare the simulation results to real world installations in the near future.

7 ACKNOWLEDGEMENTS

The authors are grateful for the project advising and funding by the Swiss Federal Office of Energy SFOE in the frame of the project SOFOWA. They acknowledge the support of the component manufacturers Viessmann Werke GmbH & Co. KG and isocal HeizKühlsysteme GmbH. The project contributes to the IEA SHC Task 44 / HPP Annex 38 “Solar and heat pumps”. The permission of Meteotest for using Meteonorm climate data for simulations within the IEA SHC Task 44 / HPP Annex 38 is gratefully acknowledged

8 REFERENCES

Dott R, Haller MY, Ruschenburg J, Ochs F, Bony J. 2011. "Reference Buildings Description of the IEA SHC Task 44 / HPP Annex 38".

Frank E. 2007. "Modellierung und Auslegungsoptimierung unabgedeckter Solarkollektoren für die Vorerwärmung offener Fernwärmenetze," Kassel University Press.

Frank E, Haller M, Herkel S, Ruschenburg J. 2010. "Systematic classification of combined solar thermal and heat pump systems," Proceedings of the International Conference on Solar Heating, Cooling and Buildings 2010; Graz, Austria.

Haller MY, Dott R, Ruschenburg J, Ochs F, Bony J. 2011. "The Reference Framework for System Simulations of the IEA SHC Task 44 / HPP Annex 38".

Malenkovic I, Eicher S, Bony J. 2012. "Definition of Main System Boundaries and Performance Figures for Reporting on SHP Systems".

Winteler C, Dott R, Afjei T, Hafner B. 2014. "Seasonal performance of a combined solar, heat pump and latent heat storage system," Energy Procedia, to be published.